Received: 6 February 2020 | Revised: 11 June 2020 | Accepted: 22 June 2020

DOI: 10.1002/app.49639

ARTICLE

Applied Polymer SCIENCE WILEY

A comparative experimental study of the hygroscopic and mechanical behaviors of electrospun nanofiber membranes and solution-cast films of polybenzimidazole

Oksana Zholobko[1] | Xiang-Fa Wu[1] | Zhengping Zhou[1] | Ted Aulich[2] | Jivan Thakare[2] | John Hurley[2]

[1]Department of Mechanical Engineering, North Dakota State University, Fargo, North Dakota

[2]Energy and Environmental Research Center, University of North Dakota, Grand Forks, North Dakota

Correspondence
Oksana Zholobko and Xiang-Fa Wu, Department of Mechanical Engineering, North Dakota State University, Fargo, ND 58108.
Email: oksana.zholobko@ndsu.edu (O. Z.); xiangfa.wu@ndsu.edu (X.-F. W.)

Funding information
DOE Office of Energy Efficiency and Renewable Energy, Grant/Award Number: DEEE0008324; Renewable Energy Program of the Industrial Commission of North Dakota; National Science Foundation, Grant/Award Number: CMMI-1234297; NDSU Development Foundation, Grant/Award Numbers: FAR0021589, FAR0031220

Abstract

This article reports a comparative experimental study of the hygroscopic and mechanical behaviors of electrospun polybenzimidazole (PBI) nanofiber membranes and solution-cast PBI films. As-electrospun nonwoven PBI nanofiber mats (with the nanofiber diameter of ~250 nm) were heat-pressed under controlled temperature, pressure and duration for the study; lab-made solution-cast PBI films and commercially available PBI films (the PBI Performance Product Inc., Charlotte, NC) were used as the control samples. Thermogravimetric and microtensile tests were utilized to characterize the hygroscopic (moisture absorption) and mechanical properties of the PBI nanofiber membranes at varying heat-pressing conditions, which were further compared to those of solution-cast PBI films. Experimental results indicated that the PBI nanofiber membranes carried slightly higher thermal stability and less hygroscopic properties than those of solution-cast PBI films. In addition, heat-pressing conditions significantly influenced the mechanical properties of the resulting PBI nanofiber membranes. The stiffness and tensile strength increase with increasing either the heat-pressing pressure or duration, and relevant mechanisms were explored. The present study provides a rational understanding of the hygroscopic and mechanical behaviors of electrospun PBI nanofiber membranes and solution-cast PBI films that are beneficial to their reliable cutting-edge applications in high-temperature filtration, polymer electrolyte membranes (PEMs), etc.

KEYWORDS

adsorption, mechanical properties, structure-property relationships, thermal properties

1 | INTRODUCTION

Hygroscopic and mechanical properties are fundamental to design, synthesis and deployment of polymeric materials for structural and multifunctional applications. The former defines the capability of moisture absorption and adsorption of a material from surrounding; the latter determines a material's load-carrying capability. Among a broad family of high-performance polymers, polybenzimidazole (PBI) carries high thermal stability with its glass transition temperature T_g in the range of 425–436°C, excellent chemical resistance, and sound

retention of mechanical properties (e.g., the stiffness and mechanical strength) in a wide range of temperature due to its unique aromatic nuclei.[1] In general, PBI represents a wide spectrum of amorphous thermoplastic aromatic heterocyclic polymers comprising benzimidazole units; meanwhile PBI also specifically refers to the commercial products coined with the trademark Celazole® (the PBI Performance Products Inc., Charlotte, NC), that is, poly 2,2′-m-(phenylene)-5,5′-bibenzimidazole as shown in Figure 1. This specific PBI is also called as *m*-PBI since the phenylene ring is meta-coordinated, and in the bulk state it carries the tensile strength of 160 MPa, Young's modulus of 5.9 GPa, and elongation of 3%. Due to its thermal stability, PBI is considered as an excellent candidate polymer for fabricating high-performance protective apparels, such as firefighter's gear, astronaut space suits, high-temperature protective gloves, aircraft wall fabrics, etc.,[2,3] in which spinning PBI into various fibrous materials with controlled fiber diameter and morphology is crucial.

In addition, PBI is a linear amorphous polymer with a high affinity for moisture due to the intermolecular hydrogen bonds between water and nitrogen atoms and the N-H groups in PBI.[4] PBI exhibits remarkable moisture regain ability up to 15–19% by weight, corresponding to three water molecules per repeat unit of PBI. The water absorption of PBI is comparable to that of cotton (16%) and the absorbed water in PBI does not leave until the temperatures are well above 150°.[2,5] Two possible molecular mechanisms are identified to be responsible for the high moisture absorption. The first is induced by two water molecules that are attached to each imidazole ring; the second is due to one water molecule that is attached to neighboring imidazole rings on adjacent polymer chains.[4] The effects of water absorption on PBI are the same as for other thermoplastic polymers, which can change the PBI dimensions, exacerbate the effects of thermal and pressure, and reduce the mechanical strength. For instance, the compressive strength of PBI is more than halved in the wet state compared to that in the dry state, and the dynamic modulus for a wetted PBI is also reduced to about half that of the dry PBI at room temperature. In addition, 10% water absorption in PBI can result in 25–30% reduction in its tensile strength.[4] The

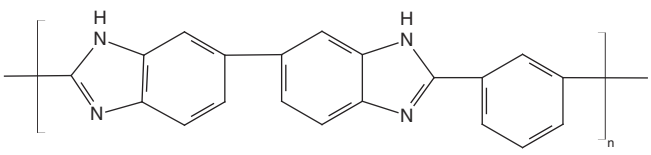

FIGURE 1 Poly 2,2′-m-(phenylene)-5,5′-bibenzimidazole (m-PBI)

absorbed moisture also influences the electrical insulation resistance and dielectric properties.[6] In addition, PBI can also be used as excellent thermal resistant coatings with a low friction surface for protection from mechanical abrasion, low coefficient of thermal expansion (similar to aluminum), high thermal and electrical insulation, and exceptional corrosion resistance to chemical attack in a wide range of substrate.[6]

Moreover, acid-doped PBI membranes are also under intensive investigation as promising proton exchange membranes (PEMs) for use in intermediate- and high-temperature fuel cells and other electrochemical devices.[7,8] In this case, the PBI membranes are commonly doped with phosphoric acids and other acids to form strong hydrogen-bond paths across the membranes for excellent proton conductivity (up to 0.2 S/cm). Organophosphonic acids are also commonly used for such purpose such as phenylphosphonic and akylphosphonic acids, among others.[9] Nevertheless, owing to the rigid-rod chain structure of PBI, the processability of PBI is poor. Typical methods for processing PBI fibers and films are based mainly on PBI solutions, such as fiber fabrication by means of dry-spinning, wet-spinning, and dry-jet wet-spinning as well as film/coating processing by means of solution-casting, dip coating, spray coating, etc. Commonly used solvents for dissolving PBI include sulfuric acid, dimethylformamide (DMF), dimethyl sulfoxide (DMSO), and dimethyl acetamide (DMAc), while DMAc is the most common used for dry-spinning PBI microfibers and solution-casting PBI films.[1]

On the other hand, with recent development of nanotechnology, the low-cost electrospinning technique has been used extensively for producing continuous nanofibers of various polymers and polymer-derived carbon, silicon, metals, metal oxides, ceramics, and so on.[10–15] Due to their unique advantages including the favorable continuity, high surface area to volume ratio, superior mechanical strength, and tunable surface morphology and microstructures, electrospun nanofibers have been finding rapidly expanding applications in high-grade gas and liquid filtration, nanocomposites, wound dressing, tissue scaffolding, drug delivery, and energy harvesting, conversion and storage, among others.[15–31] The schematic electrospinning process is shown in Figure 2, which can be conveniently extended to needleless electrospinning for scale-up continuous nanofiber production.[32–41] In the past two decades, continuous PBI nanofibers have been successfully fabricated by electrospinning for exploring their innovative applications in various cutting-edge fields, in particular PEMs for use in intermediate- and high-temperature fuel cells. Among others, Kim and Reneker[42] were the pioneers to

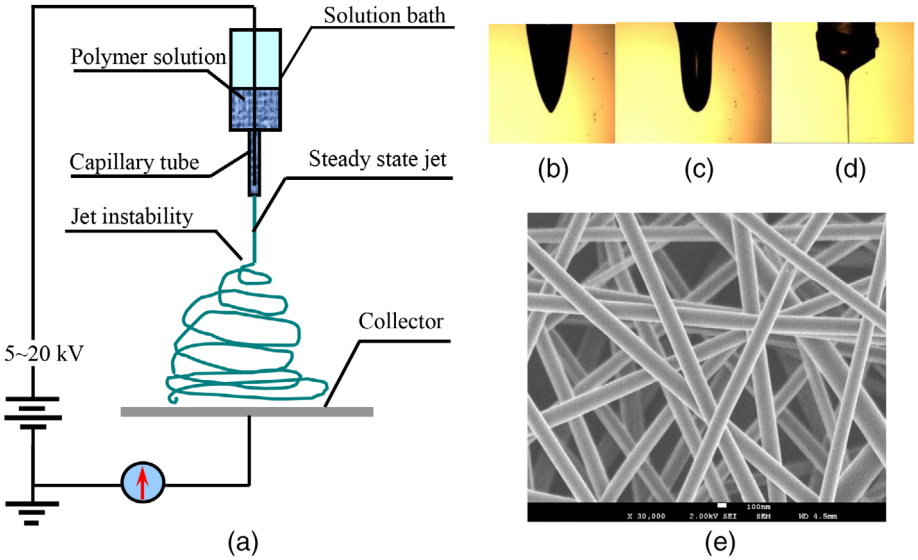

FIGURE 2 electrospinning process for continuous nanofiber fabrication: (a) schematic electrospinning setup, (b) taylor cone (deformed droplet in electrostatic field), (c) stretched droplet in electrostatic field, (d) straight jet in a stable electrospinning process, and (e) nonwoven continuous polyacrylonitrile (PAN) nanofibers collected on a fiber collector [Copyright (2020) of Institute of Physics][39] [Color figure can be viewed at wileyonlinelibrary.com]

fabricate first continuous PBI nanofibers with the fiber diameter of ~160–300 nm by electrospinning based on a PBI/DMAc solution (with the PBI and LiCl mass concentrations of ~20% and ~4%, respectively) provided by the Celanese Co. (Charlotte, NC). The resulting nonwoven PBI nanofiber mat was rinsed with a non-solvent (methanol) to remove the residual solvent (DMAc) and LiCl, followed by washing in sulfuric acid that was diluted to 50 wt. % with water to provide stabilization against shrinkage during heat treatment and to increase the mechanical strength. In addition, Kim et al.[43] fabricated continuous PBI nanofibers with the diameter of ~250 nm by electrospinning a lab-made PBI/DMAc solution that was prepared via dissolving 20 wt. % PBI in DMAc at 185°C under continuous and gentle stirring for 4 hr. The PBI nanofibers with well uniform diameters and smooth surface were used as the precursor to prepare carbon nanofibers (CNFs) via pyrosis at 700–850°C. The resulting continuous CNFs with the average pore size of 0.64–0.66 nm and the specific area of 500–1,220 m^2/g were assembled as supercapacitor electrodes with the specific capacitance up to 125–178 F/g. More recently, nonwoven PBI nanofiber membranes prepared by electrospinning have been under intensive investigation as promising PEMs, after doping with phosphoric acid, for use in intermediate- and high-temperature fuel cells.[44–47] For instance, the proton conductivity of acid-doped nonwoven PBI nanofiber membranes can reach as high as 0.17 S/cm at 160°C under anhydrous condition.[45] In these applications, the highly porous nonwoven PBI nanofiber mats with high specific surface area can provide the advantage for fast, uniform acid-doping as the liquid acids can quickly fill into the pores and diffuse into the PBI nanofibers, and the unique nanofibrous structures provide ultrafast surface proton conduction.[47] Due to the porous nanofibrous structures, high thermal and chemical stability, and excellent wettability, electrospun PBI nanofiber membranes have also been under intensive investigations for developing high-temperature, flame-retardant lithium-ion battery (LIB) separators for better thermal dimensional stability, electrochemical stability, ionic conductivity, and interfacial compatibility with electrodes to enhance the safety and electrical performance of high-energy-density LIBs.[48,49] Other advanced applications of electrospun PBI nanofibers include tissue scaffolding for neural stem cell culturing due to their porous structures, biocompatibility, and non-toxicity,[50] and selective removal of particular chemical compounds,[51] among others. Recent experimental research has also been made to improve the electrospinning conditions for PBI nanofiber fabrication, such as replacing the commonly used organic solvent DMAc by environmentally friendly and cheap ethanol/potassium hydroxide (Ethanol/KOH).[52] An increasing number of research investigations are expected in the near future for controllable PBI nanofiber fabrication and advanced multifunctional applications.

Yet, no work has been reported in the literature on systematic study of the hygroscopic and mechanical behaviors of electrospun PBI nanofiber membranes though these properties are fundamental to their potential structural and multifunctional applications. This evoked the present comparative experimental study as PBI nanofiber membranes are expected to play crucial rules in developing innovative intermediate- and high-temperature PEMs with high proton conductivity for electrochemical energy conversion and storage. After the brief introduction above, the rest of the paper is prepared in the following. In Section 2, all the materials as well as fabrication and testing methods of electrospun PBI

nanofibers and solution-cast PBI films, adopted in this study, are introduced. In Section 3, we focus mainly on dependencies of the mechanical properties of heat-pressed PBI nanofiber membranes upon the heat-pressing conditions (e.g., heating temperature, pressure and heating duration) and comparison of the hygroscopic and mechanical properties between heat-pressed PBI nanofiber membranes and solution-cast PBI films (both lab-made and procured). Consequently, conclusions of the present comparative experimental study are drawn.

2 | EXPERIMENTAL METHODS

2.1 | Materials

Standard PBI S26 solution provided by the PBI Performance Products Inc. (Charlotte, NC) was used and further diluted for the purpose of the present experimental study. The red-brown PBI S26 solution contains 0.7 dl/g PBI polymer (26.2% by weight, Mw = ~35,000) dissolved in DMAc (72.3% by weight) in the presence of a LiCl stabilizer (1.5% by weight). The viscosity of PBI S26 solution is 2,100 ± 200 (Poise) at room temperature. The procured PBI films with the thickness of 55 μm were provided by the PBI Performance Products Inc. (Charlotte, NC). Organic solvent DMAc anhydrous (99.8%) was purchased from the Sigma-Aldrich (St. Louis, MO) without further purification.

2.2 | Electrospinning of PBI nanofiber membranes and solution-casting of PBI films

The PBI/DMAc solution (with PBI mass concentration of 18% w/w) used for electrospinning of PBI nanofibers and solution-casting of PBI films was prepared via diluting the standard PBI S26 solution in DMAc. This solution was typically made by first blending the S26 solution (~20 ml) with the proper quantity of DMAc on an analog vortex mixer (the Cole-Parmer, Vernon Hills, IL) for a couple of minutes, followed by magnetic stirring at room temperature for over 12 hours.

A conventional single-needle based electrospinning setup (as illustrated in Figure 2a) was utilized for fabricating continuous PBI nanofibers. The electrospinning setup consists of a high-voltage direct-current (DC) power supply (the Gamma High Voltage Research Inc., Ormond Beach, FL) with a positive voltage output, a capillary spinneret (a tapered stainless steel needle of size 20G, McMaster-Carr, Elmhurst, IL), a digitally controlled syringe infusion pump (Cole-Parmer, Vernon Hills, IL), and a lab-made rotary drum nanofiber-collector with both the drum longitudinal and circumferential lengths of 12 in.. During a typical electrospinning test for PBI nanofiber fabrication, the solution feeding rate was set as 0.3 ml/h, the DC voltage between the spinneret (positive) and the nanofiber collector (grounded) was set as 20–25 kV, the spacing between the spinneret and the nanofiber collector was fixed at ~20 cm, and the rotating rate of the nanofiber collector was set at ~150–300 rpm. The resulting nonwoven PBI nanofibers were collected on an aluminum (Al) foil that was attached onto the collector drum by adhesive tape at its edges. Experimental observations showed that the above electrospinning setup and choices of the material and process parameters were able to sustain the stable jetting for hours without noticeable beading. After electrospinning, the Al-foil covered with nonwoven PBI nanofibers was detached from the drum nanofiber-collector and rinsed in deionized (DI) water for a few minutes for the purpose of easy peel-off of the PBI nanofiber mat from the Al-foil and removal of the residual solvent DMAc as well as the stabilizer LiCl.

The solution-casting process for PBI film fabrication (as illustrated in Figure 3) was performed via casting the PBI/DMAc solution (with PBI mass concentration of 18%) onto a flat steel panel (Q-panel, the Q-Lab Co., Westlak, OH) using a drawdown bar (the Paul N. Gardner Co., Pompano Beach, FL) with the adjustable wet layer thickness and width according to the specific designation of the drawdown bar. The as-cast PBI film (attached onto the steel panel) was further baked in an air-circulating oven above 100°C for a few minutes to evaporate sufficient amount of the solvent DMAc. Furthermore, the solution-cast PBI film (on the steel panel) was rinsed in DI water to remove the residual solvent DMAc and the stabilizer LiCl and then peeled gently off the steel panel. Finally, after annealed in the oven above 100°C for another ~1 min, the free-standing PBI film was ready for thermogravimetric and mechanical characterizations in the present study.

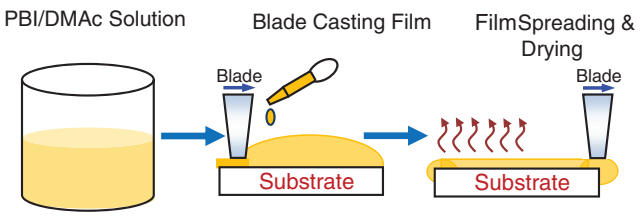

FIGURE 3 Schematic representation of a solution-casting process for PBI film fabrication [Color figure can be viewed at wileyonlinelibrary.com]

2.3 | Heat-pressing of electrospun PBI nanofiber membranes

As-electrospun PBI nanofiber mats consisted of randomly deposited PBI nanofibers with a large portion of pores and less fiber-fiber interaction. As a matter of fact, the load-carrying capability of such loosely assembled nanofiber networks is very low due to the easy fiber-fiber sliding and the resulting weak load transfer from fiber to fiber when subjected to in-plane external loading.[53–55] In this case, the individual fibers of the fiber network respond to external loads nearly independently.[56–68] Heat-pressing is a low-cost and effective method that can be utilized to improve the global mechanical properties of electrospun nanofiber mats via enhancing the fiber-fiber interaction and fusion under combined heating (thermal activation) and compressive stressing as well as significantly reducing the size of pores and voids between fibers.[20,53–55] In the present study, the temperature utilized in the heat-pressing process was fixed at 200°C while two pressures of 1.918 MPa and 3.068 MPa and three heating durations of 1, 5, and 20 min were adopted, respectively, to examine dependencies of the mechanical properties of the resulting PBI nanofiber membranes upon the heat-pressing process parameters (i.e., the pressure and duration in this study). Choices of the heat-pressing parameters (i.e., the heating temperature and pressure) were based on the availability of the hot-press machine in the affiliated university, and selection of three heating durations (i.e., 1, 5, and 20 min) was to examine the effect of heating duration on the mechanical properties of the resulting heat-pressed PBI nanofiber membranes. The heat-pressing treatment was performed on a 15-tone hydraulic hot-press installed with an electrical heating unit (the Carve Inc., Wabash, IN). During a heat-pressing process, a PBI nanofiber mat sample with the areal size about 100 mm × 100 mm was sandwiched between two Al-foils, and then the sandwiched PBI/Al-foil assembly was further sandwiched between two stainless steel plates with finely polished mirror-like surfaces and the dimensions of 152.4 mm × 152.4 mm × 12.7 mm. Herein, the time duration for the heat-pressing process was defined as the holding time once the heating temperature reached the targeted temperature of 200°C. After the holding time, the electrical heating unit of the hot-press was turn off and the pressed PBI nanofiber membrane sample was cooled down in ambient to the room temperature. For the convenience of peeling off the heat-pressed PBI nanofiber membrane sample from the Al-foils, the sandwiched PBI/Al-foil assembly was first wetted in water and then the PBI nanofiber membrane sample was gently peeled off. The thickness of the heat-pressed PBI nanofiber membranes and solution-cast PBI films was typically around 35 to 50 μm (42.5 ± 7.5 μm) depending on the initial thickness of the PBI nanofiber mat. The thickness of procured PBI films adopted in the present experimental study was 55 μm.

2.4 | SEM-based microstructural characterization of as-electrospun PBI nanofibers, heat-pressed PBI nanofiber membranes, and solution-cast PBI films

Typical samples of as-electrospun and heat-pressed PBI nanofiber membranes were collected for characterization of their surface morphologies and fiber diameters by using an FE-SEM (JEOL JSM-7600F, JEOL Ltd., Japan) and attached image processing software package. For the purpose of comparison, the surface morphologies of lab-made solution-cast and procured PBI films were also characterized by SEM. In attempt to characterize the cross-sectional morphologies of solution-cast and procured PBI films, the cross-sectional surfaces of these samples were generated via fracturing (bending) the fragile film samples after fast liquid-nitrogen quenching. Prior to SEM characterization, all the PBI samples were first sputter-coated with carbon to avoid possible charge accumulation onto the samples during the SEM characterization.

2.5 | Thermogravimetric and mechanical characterization

Small pieces of samples used for thermogravimetric analysis (TGA) were cut from as-electrospun PBI nanofiber mat, heat-pressed PBI nanofiber membranes at varying heat-pressing conditions (e.g., the pressure and heating duration), and lab-made and procured solution-cast PBI films for determining and comparing their hygroscopic behaviors from room temperature to 350°C. The TGA tests were performed using a thermogravimetric analyzer TGA 5500 (the TA Instruments, New Castle, DE) based on a standard TGA operating procedure for thermal stability assessment of all the PBI nanofiber membrane and film samples as follows. The tested sample was first heated from room temperature (~22°C) to 300°C at a heating rate of 5°C/min under N_2 atmosphere and maintained at 300°C for 2 hr, and then further heated up to 350°C at the same heating rate of 5°C/min and finally maintained the sample at 350°C for another 2 hr under N_2 atmosphere.

Instron 5542 Tensile Tester installed with a computerized digital data acquisition system (with the maximum

load-carrying capacity 100 N) was employed for characterization and comparison of the mechanical properties of heat-pressed PBI nanofiber membranes, solution-cast PBI films, and procured PBI films. The ASTM D882-18 standard test method[69] for tensile properties of thin plastic sheeting was followed in this test. For heat-pressed PBI nanofiber membranes, six combinations of the heat-pressing conditions, including pressures of 1.92 and 3.07 MPa and heating durations of 1, 5, and 20 min, were considered, respectively. Rectangular microtensile test specimens with the areal size of 10 mm × ~70 mm and thickness of 35–50 μm (42.5 ± 7.5 μm) were scissored cautiously from the PBI membrane and film samples to avoid any predamages at the sample edges; plastic adhesive tabs (cut from a 3 M Scotch® foam mounting double-sided tape) with the areal size of 10 mm × 10 mm were firmly attached onto the two ends at two sides of each microtensile test specimen to avoid pre-mature failure at the fixture regions. Thus, the nominal/effective areal size of the tensile test specimens was 10 mm × 50 mm as shown in Figure 4. During a uniaxial tensile test, displacement-control method with the loading rate of 2 mm/min was maintained and at least three specimens were tested in each case of the PBI specimens of either PBI membranes at a particular heat-pressing condition or solution-cast and procured films. A tension test with the specimen ultimate failure occurring between the upper and lower tabs was regarded as a successful tension test, and the corresponding load–displacement diagram was recorded for data reduction to extract the mechanical properties of the specimen.

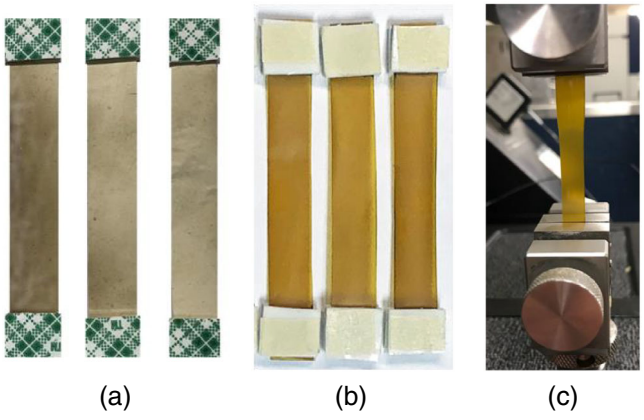

FIGURE 4 Rectangular microtensile test specimens and uniaxial microtensile test setup: (a) Heat-pressed PBI nanofiber membrane specimens (Dimensions: 10 mm × 50 mm × 42.5 μm); (b) procured PBI film specimens (Dimensions: 10 mm × 50 mm × 55 μm); and (c) a microtensile test setup (installed with a PBI film specimen in tension) [Color figure can be viewed at wileyonlinelibrary.com]

3 | RESULTS AND DISCUSSION

3.1 | Microstructures and morphologies of PBI nanofibers, heat-pressed PBI nanofiber membranes and solution-cast PBI films by SEM

Figure 5 shows the low- and high-magnification SEM micrographs of typical as-electrospun PBI nanofibers, from which it can be found that the as-electrospun PBI nanofiber mat is well nonwoven and highly porous though the PBI nanofibers were collected using a rotary drum nanofiber collector. The PBI nanofibers of the mat are well uniform with the diameter of ~250 nm and no obvious beads are detected from the SEM micrographs. Thus, the present material (18 wt.% PBI/DMAc) and process parameters (Spinneret needle size: 20G; solution feeding rate: 0.3 ml/h; DC voltage: ~22 kV; spacing between the spinneret and nanofiber collector: ~20 cm) adopted in the electrospinning test can lead to high-quality continuous PBI nanofibers. Yet, in order to maintain the stable jetting condition in electrospinning, the low solution feeding rate of 0.3 ml/h had to be adopted in this case. Such a solution feeding rate is quite low and inefficient for large-scale PBI nanofiber fabrication. To enhance the PBI nanofiber productivity, in this study we also tested to induce a tubular airflow via assembling a lab-made airflow nozzle (via 3D-printing) that surrounded the spinneret. It was found that when applying the tubular airflow pressure of 4–10 psi (27.6–70 kPa) and the same material and process parameters as adopted in the electrospinning test above, the solution feeding rate can be increased 10 times without noticeable jet beading. In addition, our test also showed that a pure tubular airflow without applying a DC voltage cannot form a stable jet. Thus, the airflow-assisted electrospinning method can be potentially adopted as a high-efficiency, robust technique for low-cost, mass fabrication of continuous PBI nanofibers and other types of polymer nanofibers including continuous core-shell nanofibers.

Figure 6 shows the typical surface and cross-sectional morphologies of the PBI nanofiber membranes after heat-pressing under the process conditions of heating temperature of 200°C, pressure of 1.918 MPa, and heating duration of 1 min. Compared to Figure 5, it can be found that the size of pores and voids in this heat-pressed PBI nanofiber membrane (See Figure 6) was decreased significantly, and the fiber-fiber interaction and fusion were enhanced. This observation is similar to other heat-pressed polymer nanofiber membranes based on cellulose acetate, polyvinylidene fluoride (PVDF) and other thermoplastic polymers for water filtration and

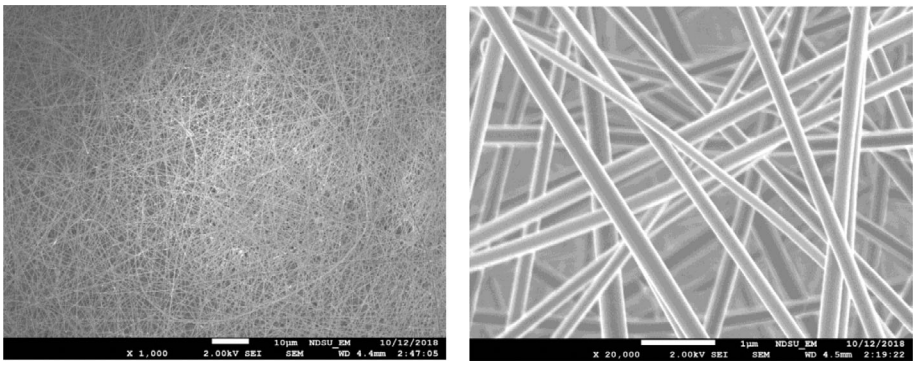

FIGURE 5 Low- and high-magnification (×1,000 and ×20,000) SEM micrographs of as-electrospun continuous monolithic PBI nanofibers with diameters of ~250 nm

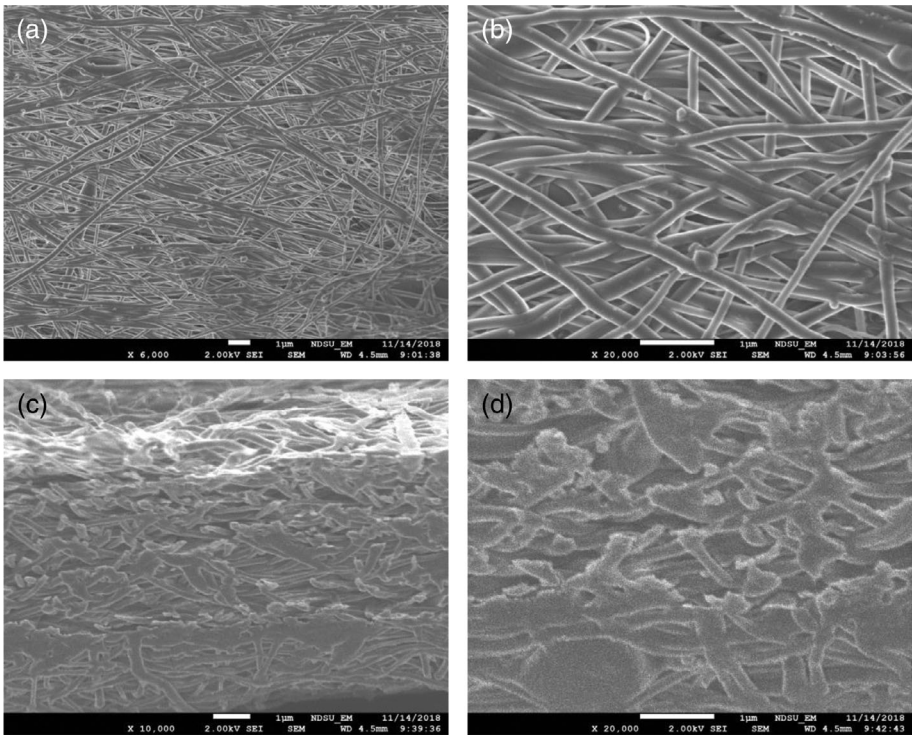

FIGURE 6 SEM micrographs of a typical PBI nanofiber membrane after heat-pressing (Processing condition: Pressure 1.92 MPa, temperature 200°, and duration 1 min). Panels (a) and (b): Membrane surface morphologies; Panels (c) and (d): Membrane cross-sectional morphologies

distillation,[20,68] among others. Correspondingly, the mass density, gas/liquid impermeability, and mechanical properties (e.g., the elastic modulus and tensile strength) of the heat-pressed PBI nanofiber membranes are expected to improve greatly. In addition, Figure 6 also indicates the existence of obvious fibrillar features and patterns as well as small pores inside the membrane after heat-pressing, that is, the thermoplastic PBI nanofibers were not completely fused by the heat-pressing process under the present processing conditions. This is true since T_g of PBI is as high as 425°C, which is much higher than the heat-pressing temperature of 200°C as adopted in this study. Such a phenomenon was also observed in other heat-pressed PBI nanofiber membranes in the present study with the heat-pressing pressures of 1.92 and 3.07 MPa and the heating durations of 1, 5, and 20 min, respectively, and no noticeable visual differences can be identified from the membrane morphologies within the present heat-pressing conditions. Such porous PBI nanofiber membranes can provide tunable gas/liquid permeability for high-efficiency filtration, fast acid-doping of PBI-based PEMs, etc.

Figures 7 and 8 show the SEM micrographs of the surface and cross-sectional morphologies of lab-made solution-cast and procured PBI film samples. It can be found that the surface morphologies (See Figure 7) of lab-made solution-cast PBI film contain relatively oriented features and scratches with the feature heights in the submicron scale on the surface, which were induced by the one-directional motion of the drawdown bar during the solution casting process. As the solvent evaporation was well controlled, no obvious pinholes and surface roughness due to liquid film instability were detected. Figure 7 also shows the well uniform cross-sectional

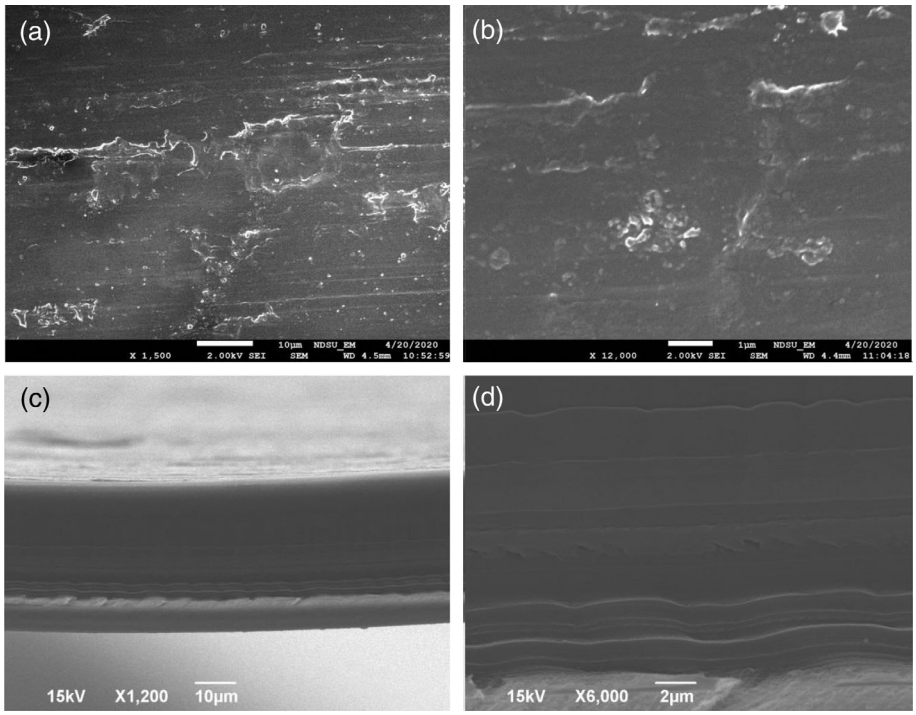

FIGURE 7 SEM micrographs of a lab-made solution-cast PBI film. Panels *A* and *B*: Film surface morphologies; Panels *C* and *D*: Film cross-sectional morphologies

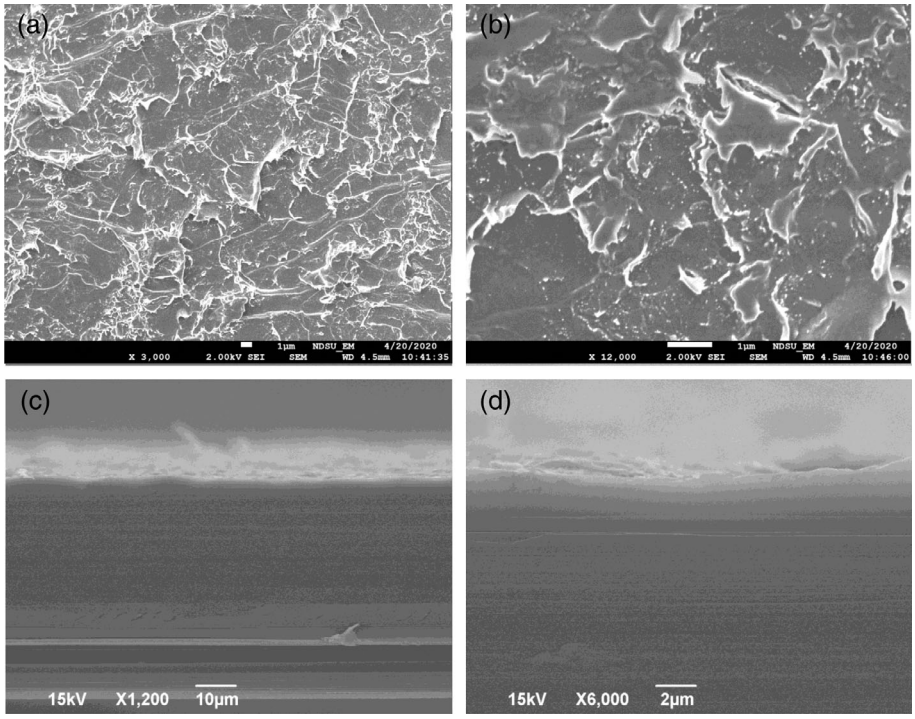

FIGURE 8 SEM micrographs of a procured PBI film. Panels (a) and (b): Film surface morphologies; Panels (c) and (d): Film cross-sectional morphologies

morphologies of the lab-made PBI film without obvious cavitation and inclusions though seemingly layered microstructures are detected that might be related to drying-induced solvent gradient across the film or the SEM sample preparation via fracturing (bending) the fragile PBI film sample after fast liquid-nitrogen quenching. The SEM characterization in Figure 7 evidences the high quality of the lab-made solution-cast PBI films. In addition, the surface morphologies of procured PBI film (See Figure 8) show the obvious random spike-shaped microstructural features that can be related to the dry detachment of the PBI film from the substrate during the industrial fabrication process. Figure 8 also shows that the procured PBI films carry fine uniform

cross-sectional morphologies without obvious cavitation and inclusions similar to those of lab-made PBI films (See Figure 7), which indicate the potentially similar mechanical performances of both the PBI films.

3.2 | Thermogravimetric behavior of as-electrospun nanofibers, heat-pressed PBI nanofiber membranes, and solution-cast PBI films

Figures 9–12 show the typical thermogravimetric behaviors of as-electrospun PBI nanofibers (prior to heat-pressing), heat-pressed PBI nanofiber membranes, lab-made solution-cast PBI films, and procured PBI films. The TGA temperature program is shown in Panel (a) of Figures 9–12, which includes four stages: (1) The sample is heated from room temperature (~22°C) to 300°C at a heating rate of 5°C/min under N_2 atmosphere; (2) The temperature is maintained at 300°C for 2 hr to remove all moisture and solvent of the sample; (3) The sample is further heated up to 350°C at the same heating rate of 5°C/min; (4) The sample is maintained at 350°C for another 2 hr. The choice of temperature 350°C as the upper temperature limit was based on the potential use of the PBI nanofiber membranes and films as intermediate- and high-temperature PEMs with the work temperature around or below 300°C.

For as-electrospun PBI nanofiber samples, TGA results shown in Figure 9b indicate that the mass loss in the first ramp heating stage up to 300°C is ~7%, which mainly includes absorbed moisture and residual solvent DMAc. In the rest three heating stages after reaching 300°C, the mass loss of the PBI nanofibers is only ~2% for over 4 hr, which evidences the excellent thermal stability of the electrospun PBI nanofibers. For heat-pressed PBI nanofiber membrane samples (Heat-pressing conditions of pressure 1.918 MPa and heating duration 20 min.), TGA results shown in Figure 10b demonstrate that the mass loss in the first ramp heating stage up to 300°C is ~12%, which mainly includes absorbed and residual solvent DMAc. In the rest three heating stages after reaching 300°C, the mass loss is only ~2% for over 4 hr, which again evidences the excellent thermal stability of the heat-pressed PBI nanofibers membranes. Compared to as-electrospun PBI nanofiber sample (See Figure 9b), the higher mass loss (~12%) in the first ramp heating stage of the heat-pressed PBI nanofiber membrane samples may be related to the nearly saturated moisture absorption from environment after heat-pressing (as the samples had been stored in lab for a quite long time). Nevertheless, the nearly same mass loss of the above two samples after heating at 300°C indicates that heat-pressing does not noticeably influence the thermal stability of electrospun PBI nanofibers.

Figure 11b shows that the mass loss of a lab-made solution-cast PBI film sample in the first ramp heating state is ~22%, which is higher than the maximum moisture absorption (15–19%) of PBI as reported in the literature.[1] In the rest three heating stages after reaching 300°C, the mass loss of the PBI film sample is ~6% for over 4 hr. Herein, the PBI and solvent DMAc used in the solution-casting process are the same as those used for electrospinning PBI nanofibers. As no postprocessing was applied for the solution-cast PBI films, these PBI films were expected to carry the similar thermal stability to that of the above two PBI nanofiber samples. Therefore, the obvious deviation of the mass loss of the solution-cast PBI films from those of PBI nanofiber samples could be caused by the solvent DMAc trapped in the solution-cast PBI films. In contrast, Figure 12b shows that the mass loss of a procured PBI film sample in the first ramp heating stage is ~19%, which is close to the maximum moisture absorption rate of PBI. In the rest three heating stages after reaching 300°C, the mass loss of the PBI film is ~5% for over 4 hr, which also shows the excellent thermal stability of the PBI films. Yet, by comparison of Figure 12b with Figure 9b, it can be concluded that the PBI nanofiber samples had not reached the state of saturated moisture absorption before the TGA test. In this case, the as-electrospun PBI nanofiber mats after DI water rinsing were first dried in air and then stored in a

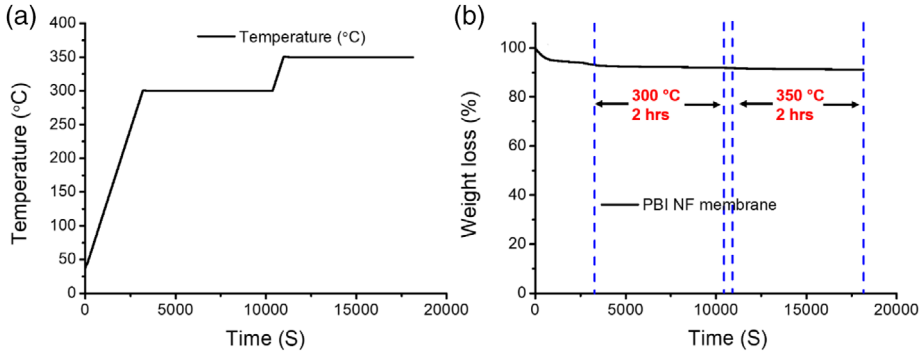

FIGURE 9 TGA-based thermal stability assessment of a typical as-electrospun PBI nanofiber mat (prior to heat-pressing): (a) TGA temperature program; (b) TGA profile, showing approximate 2% mass loss after reaching 300°C [Color figure can be viewed at wileyonlinelibrary.com]

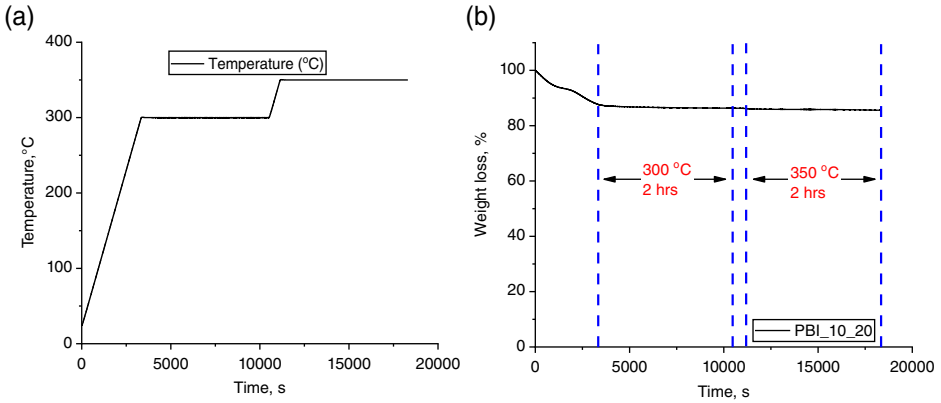

FIGURE 10 TGA-based thermal stability assessment of a typical heat-pressed PBI nanofiber membrane (Heat-pressing condition: Pressure 1.92 MPa, temperature 200°, and duration 1 min): (a) TGA temperature program; (b) TGA profile, showing approximate 2% mass loss after reaching 300°C [Color figure can be viewed at wileyonlinelibrary.com]

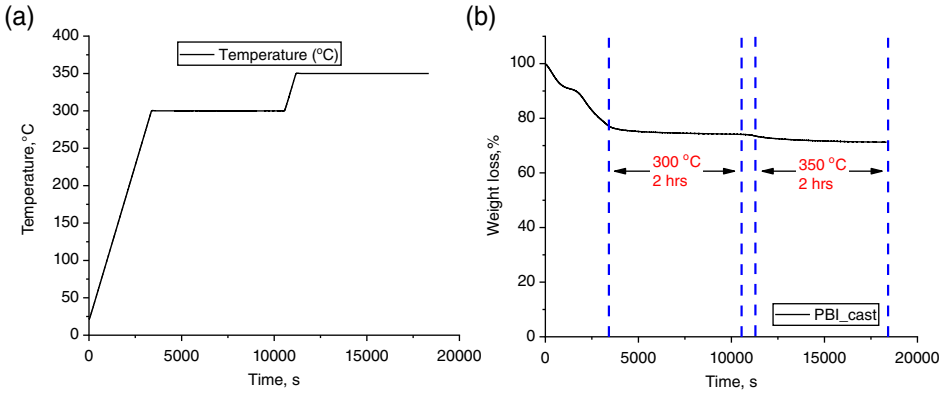

FIGURE 11 TGA-based thermal stability assessment of a typical lab-made solution-cast PBI film: (a) TGA temperature program; (b) TGA profile, showing approximate 6% mass loss after reaching 300°C [Color figure can be viewed at wileyonlinelibrary.com]

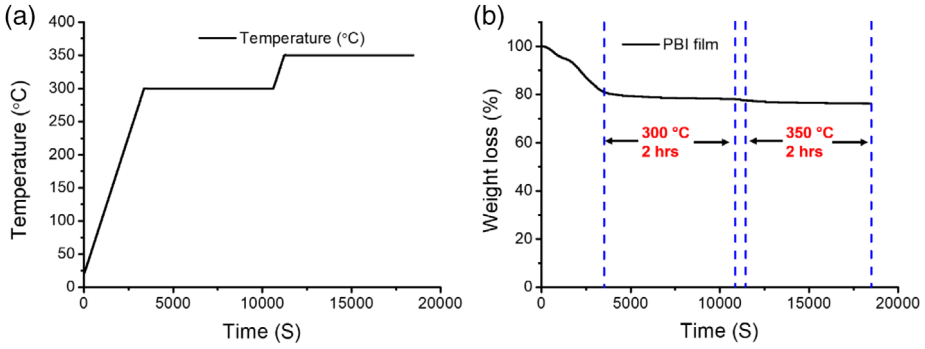

FIGURE 12 TGA-based thermal stability assessment of a typical procured PBI film: (a) TGA temperature program; (b) TGA profile showing approximate 5% mass loss after reaching 300°C [Color figure can be viewed at wileyonlinelibrary.com]

sealed storage bag. However, the procured PBI film was stored for a relatively long time, typically reaching the state of saturated moisture absorption, that is, water absorption of ~19% by mass as measured in the present study. In addition, Figure 12b also shows the total mass loss of the PBI film up to 24%, of which ~5% happened after 300°C. This observation implies that the procured PBI films had relatively less thermal stability compared to the PBI nanofiber samples. On the other hand, the procured PBI films might have been blended with a small quantity of less thermally stable polymers or other fillers to facilitate the film processing, not released by the provider yet. In summary, the TGA results indicates the high thermal stability and hygroscopic properties of as-electrospun PBI nanofibers, heat-pressed PBI nanofiber membranes, lab-made solution-cast PBI films, and procured PBI films

3.3 | Mechanical characterization of heat-pressed PBI nanofiber membranes and solution-cast PBI films

Figures 13 and 14 show a family of typical stress–strain diagrams of the PBI nanofiber membrane and film samples obtained from the microtensile tests. It can be found

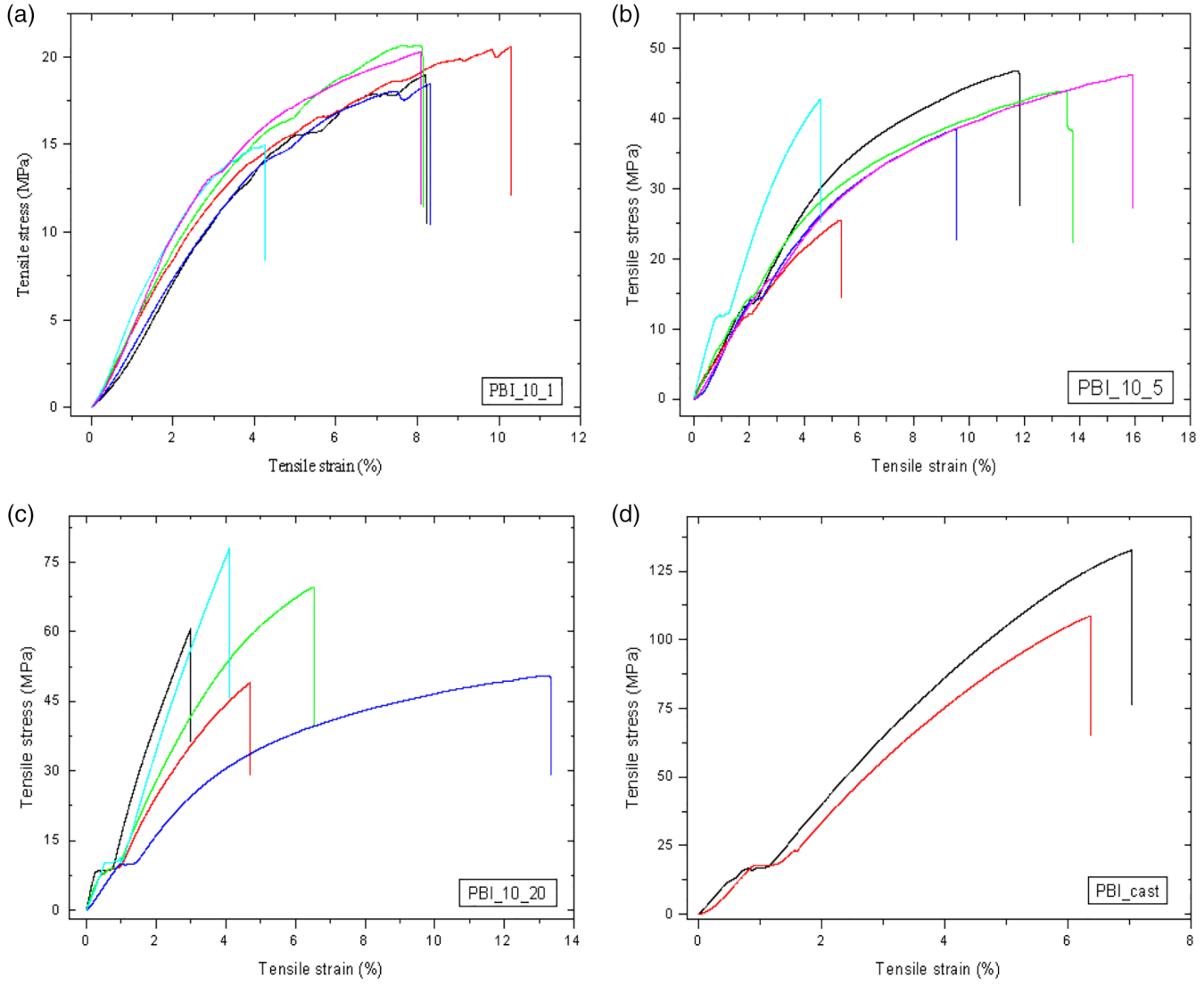

FIGURE 13 Typical tensile stress–strain diagrams of heat-pressed PBI nanofiber membrane and solution-cast film samples. (a–c): Heat-pressed PBI nanofiber membrane samples with heat-pressing conditions: Temperature of 200°C, pressure of 1.92 MPa, and heating durations of 1, 5, and 20 min, respectively; (d) Solution-cast PBI film samples [Color figure can be viewed at wileyonlinelibrary.com]

from Figure 13 that the heat-pressing conditions significantly influence the mechanical behaviors of heat-pressed PBI nanofiber membranes. Given the heating temperature of 200°C and pressure of 1.92 MPa, the elastic modulus and tensile strength increase substantially with increasing heating duration. In particular, it can be found from Figure 13a–c that the average tensile strength of the heat-pressed PBI nanofiber membranes increases from 26.37 MPa at the heating duration of 1 min to 39.19 MPa and 61.15 MPa at the heating durations of 5 and 20 min, respectively. In contrast, the corresponding average tensile strains at break decrease noticeably, that is, heat-pressed PBI nanofiber membranes become more brittle with increasing heating duration. Such observations can be rationally correlated to the thermoplastic behavior of the PBI nanofibers. With increasing heating duration, the molecular chains of amorphous PBI become more thermally activated, which leads to a higher extent of fusion between neighboring PBI nanofibers and plastic deformations of the PBI nanofiber networks due to time-dependent vigorous molecular chain motion and penetration.

In addition, the mechanical properties of heat-pressed PBI nanofiber membrane samples can also be enhanced with increasing pressure as adopted in the heat-pressing process, as summarized in Table 1 and shown in Figure 13a–c. Given the heating temperature of 200°C and heating duration of 1 min, the average tensile strength of PBI nanofiber membranes increases from 26.37 MPa at the pressure of 1.92 MPa to 45.36 MPa at the pressure of 3.07 MPa. Meanwhile, at fixed heating temperature of 200°C and duration of 5 min in

heat-pressing, the average tensile strength of the PBI nanofiber membrane samples increases from 39.19 MPa at the pressure of 1.92 MPa to 60.69 MPa at the pressure of 3.07 MPa. Such observations can be attributed to the thermal activation of the thermoplastic PBI polymer as mechanical stress/strain rate and temperature are the two dominate factors of the rate effect on the fiber-fiber fusion and therefore the mechanical stiffness and strength according to Arrhenius' law.[70–73] In addition, for porous thermoplastic PBI nanofiber networks, a higher pressure obviously results in the larger plastic deformations, that is, a reduced volume fraction of pores and voids and the higher mechanical stiffness and strength of the resulting heat-pressed PBI nanofiber membranes. Yet, at fixed heating temperature of 200°C and duration of 20 min as adopted in the heat-pressing process, Table 1 shows that the pressure of 3.07 MPa results in an obvious drop in both the average tensile strength (10.87 MPa) and the average tensile strain at break (5.20%). In this case, the high pressure and heating duration led to the fragile PBI nanofiber membranes. When subjected to tensile loading, the residual pores, voids, and premature micro edge damages in such fragile (brittle) PBI membranes induced high stress concentration and, thus, low ultimate tensile strength due to brittle fracture, but not plastic deformation.

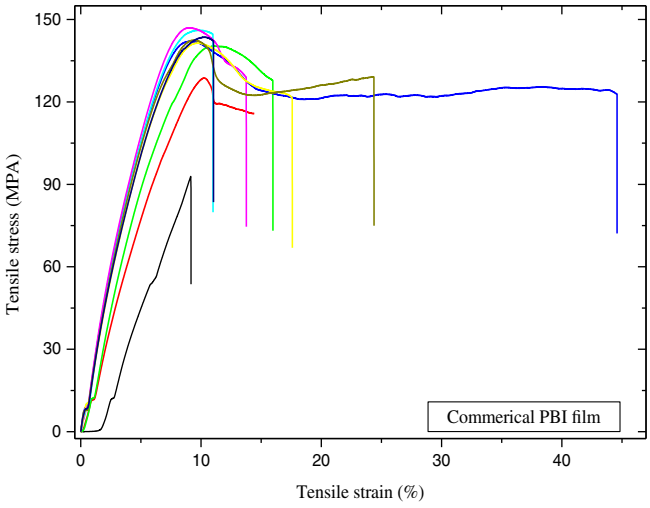

FIGURE 14 Typical tensile stress–strain diagrams of procured PBI film samples [Color figure can be viewed at wileyonlinelibrary.com]

Besides, Figures 13d and 14 show the stress–strain diagrams of lab-made solution-cast and procured PBI film samples in this study. It can be found that both the PBI films carry close stiffness and tensile strength, which are higher than those of heat-pressed PBI nanofiber membranes as both the PBI film samples carry dense microstructures without obvious pores, voids, and inclusions compared to the PBI nanofiber membrane samples, as evidenced in the SEM micrographs in Figures 6–8. Figure 15 shows the images of the PBI nanofiber membrane and film samples after microtensile failure. It was detected that all the PBI nanofiber membrane samples failed in the brittle fracture mode without obvious plastic deformations, while the PBI films failed with some extent of plastic deformations as shown in Figure 15b and in the stress–strain diagrams in Figure 14. In an exceptional case, one procured PBI film sample in this study exhibited significant plastic deformation and nonlinear wrinkling, as shown in Figure 14 with the tensile strain at break up to 45%, obvious necking and related moving plastic front, as shown in the left sample in Figure 15b. Such unique large plastic deformation, necking, and nonlinear wrinkling in PBI films have not been reported yet in the literature and in the data sheets released by the PBI Performance Products Inc. The governing mechanism of such large plastic deformation and necking could be related to the plastic blunting at the micro crack tips in the PBI film due to molecular chain reorientation and sizing under large tensile strains, which can be further explored and exploited for exceptional improvement of the ductility and toughness of PBI polymers for high-temperature structural applications.

TABLE 1 Average ultimate tensile strengths (MPa) and tensile strains at break (%) of PBI nanofiber membrane and film samples

Sample	Commercial PBI film	PBI_cast	PBI_10_1	PBI_10_5	PBI_10_20	PBI_16_1	PBI_16_5	PBI_16_20
Tensile strength (MPa)	130.08 ± 17.03	120.35 ± 16.54	26.37 ± 1.36	39.19 ± 6.62	61.15 ± 12.29	45.36 ± 10.75	60.69 ± 0.50	10.87 ± 5.88
Tensile strain at break (%)	9.81 ± 0.68	6.71 ± 0.47	8.58 ± 0.96	11.01 ± 4.29	6.33 ± 4.12	11.52 ± 2.39	5.37 ± 2.27	5.20 ± 0.75

Note: PBI_cast: Lab-made solution-cast PBI film samples; PBI_10_1, PBI_10_5, PBI_10_20: Heat-pressed PBI nanofiber membrane samples under the heat-pressing conditions:. Temperature of 200°C, pressure of 1.92 MPa (10,000-lb compressive force of the hot-press) and heating durations of 1, 5, and 20 minutes, respectively. PBI_16_1, PBI_16_5, PBI_16_20: Heat-pressed PBI nanofiber membrane samples under heat-pressing conditions: Temperature of 200°C, pressure of 3.07 MPa (16,000-lb compressive force of the hot-press) and heating durations of 1, 5, and 20 minutes, respectively.

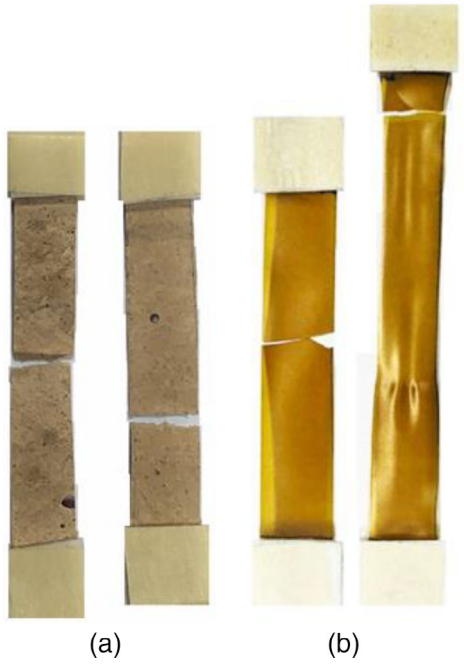

FIGURE 15 Digital images of failed tensile test samples of typical (a) heat-pressed PBI nanofiber membrane samples, and (b) procured PBI film samples [Color figure can be viewed at wileyonlinelibrary.com]

4 | CONCLUSIONS

A comparative experimental study has been conducted on the hygroscopic and mechanical behaviors of heat-pressed electrospun PBI nanofiber membranes and solution-cast PBI films. Continuous PBI nanofibers with well uniform fiber diameters were successfully fabricated by electrospinning and related airflow-assisted electrospinning technique. Heat-pressing has been employed successfully to process the PBI nanofiber membranes with intelligently controlled mechanical properties and pore size via adjusting the heating temperature, pressure, and heating duration. TGA results indicated the excellent hydroscopic property and thermal stability of heat-pressed PBI nanofiber membranes as well solution-cast and procured PBI films in the tested temperature range from room temperature to 350°C. The strain-stress diagrams of the tested PBI nanofiber membrane and film samples showed that the heat-pressing conditions significantly influenced the mechanical properties of heat-pressed PBI nanofiber membrane samples. At fixed heating temperatures, the pressure and heating duration adopted in the heat-pressing process are positively correlated to the stiffness and tensile strength of the resulting PBI nanofiber membrane samples, such that the higher the pressure or the heating duration, the higher are the stiffness and tensile strength of the resulting PBI nanofiber membranes, while the tensile strain at break decreases with increasing either the pressure or heating duration adopted in heat-pressing process.

In addition, the present microtensile test results of the PBI nanofiber membrane and film samples also show that the stiffness and tensile strength of the heat-pressed PBI nanofiber membranes are below those of solution-cast and procured PBI films. The latter can be considered as the upper limits of the mechanical properties and gas/liquid impermeability of heat-pressed PBI nanofiber membranes. Therefore, heat-pressing process can be employed and optimized for tuning the microstructural, mechanical, and physical properties of PBI nanofiber membranes for broad high-performance structural and multifunctional applications such as high-temperature gas and liquid filters, PEMs, and so on. Finally, the present experimental methodology can be further utilized for comparative studies of the hygroscopic, mechanical, electrochemical and other physical properties of other polymer nanofiber membranes and polymer films.

ACKNOWLEDGMENTS

The financial support of this research by the Office of Energy Efficiency and Renewable Energy (EERE) of the U.S. Department of Energy under the Advanced Manufacturing Office Award Number DE-EE0008324, the Renewable Energy Program of the Industrial Commission of North Dakota, the National Science Foundation (Award No.: CMMI-1234297), and the NDSU Development Foundation (Award No.: FAR0021589; FAR0031220) is gratefully acknowledged. The views and opinions of authors expressed herein do not necessarily state or reflect those of the United States Government, the Industrial Commission of North Dakota, the EERC, or any agency thereof.

ORCID

Xiang-Fa Wu https://orcid.org/0000-0003-2008-7564

REFERENCES

[1] T. S. Chung, *J. Macromol. Sci. C: Polym. Rev.* **1997**, *37*, 277.
[2] T. D. Dang, L. S. Tan, F. E. Arnold, *Polym. Prep.* **1990**, *31*, 451.
[3] https://en.wikipedia.org/wiki/Polybenzimidazole_fiber.
[4] N. W. Brooks, R. A. Duckett, J. Rose, I. M. Ward, J. Clements, *Polymer* **1993**, *34*, 4039.
[5] N. Iwamoto, *Polym. Eng. Sci.* **1994**, *34*, 434.
[6] *Celazole® PBI U-60 Moisture Management Guide*, the PBI Performance Products, Inc. **2012**.
[7] Q. Li, J. O. Jensen, R. F. Savinell, N. J. Bjerrum, *Prog. Polym. Sci.* **2009**, *34*, 449.
[8] Q. Li, D. Aili, H. A. Hjuler, J. O. Jensen, *High temperature polymer electrolyte membrane fuel cells: Approaches, status, and perspectives*, Springer: New York **2016**.
[9] Akita, H.; Ichikawa, M.; Nosaki, K.; Oyanagi, H.; Iguchi, M. US Patent 6,124,060, **2000**.
[10] D. H. Reneker, I. Chun, *Nanotechnology* **1996**, *7*, 216.
[11] R. H. Reneker, A. L. Yarin, E. Zussman, H. Xu, *Adv. Appl. Mech.* **2007**, *41*, 43.
[12] D. H. Reneker, A. L. Yarin, *Polymer* **2008**, *49*, 2387.
[13] Y. Dzenis, *Science* **2004**, *304*, 1917.

[14] D. Li, Y. N. Xia, *Adv. Mater.* **2004**, *16*, 1151.
[15] Z. M. Huang, Y. Z. Zhang, M. Kotaki, S. Ramakrishna, *Compos. Sci. Tech.* **2003**, *63*, 2223.
[16] C. Burger, B. S. Hsiao, B. Chu, *Annu. Rev. Mater. Res.* **2006**, *36*, 333.
[17] R. S. Barhate, S. Ramakrishna, *J. Membr. Sci.* **2007**, *296*, 1.
[18] V. Thavasi, G. Singh, S. Ramakrishna, *Energy Environ. Sci.* **2008**, *1*, 205.
[19] Z. Zhou, X. F. Wu, *Mater. Lett.* **2015**, *160*, 423.
[20] Z. Zhou, W. Lin, X. F. Wu, *Colloids Surface A: Physcochem. Eng. Asp.* **2016**, *494*, 21.
[21] Y. Liao, C. H. Loh, M. Tian, R. Wang, A. Fang, *Prog. Polym. Sci.* **2018**, *77*, 69.
[22] X. Zhang, L. Ji, O. Toprakci, Y. Liang, M. Alcoutlabi, *Polym. Rev.* **2011**, *3*, 239.
[23] Zhou, Z.; Wu, X. F. J. *Power Source* **2013**, *222*, 410.
[24] C. Lai, Z. Zhou, L. Zhang, X. Wang, Q. Zhou, Y. Zhao, Y. Wang, X. F. Wu, Z. Zhu, H. Fong, *J. Power Sources* **2014**, *247*, 134.
[25] Z. Zhou, X. F. Wu, H. Hou, *RSC Adv.* **2014**, *4*, 23622.
[26] Z. Zhou, S. Sigdel, J. Gong, B. Vaagensmith, H. Elbohy, H. Yang, S. Krishnan, X. F. Wu, Q. Qiao, *Nano Energy* **2016**, *22*, 558.
[27] B. Zhang, F. Kang, J. M. Tarascon, J. K. Kim, *Prog. Mater. Sci.* **2016**, *76*, 319.
[28] X. F. Wu, Y. A. Yarin, *J. Appl. Polym. Sci.* **2013**, *130*, 2225.
[29] X. F. Wu, A. Rahman, Z. Zhou, D. D. Pelot, S. Sinha-Ray, B. Chen, S. Payne, A. L. Yarin, *J. Appl. Polym. Sci.* **2013**, *129*, 1383.
[30] S. Mohammadzadehmoghadam, Y. Dong, I. J. Davies, *J. Poym. Sci. B: Polym. Phys.* **2015**, *53*, 1171.
[31] X. F. Wu, O. Zholobko, Z. Zhou, A. Rehman, *Electrospun polymer and composites: Ultrafine materials, high performance fibers and wearables*, Woodhead Publishing Ltd., Cambridge, UK, **2020**, p. 200.
[32] A. L. Yarin, E. Zussman, *Polymer* **2004**, *45*, 2977.
[33] X. F. Wu, Y. A. Dzenis, *J. Phys. D: Appl. Phys.* **2005**, *38*, 2848.
[34] D. Lukas, A. Sarkar, P. Pokorny, *J. Appl. Phys.* **2008**, *103*, 084309.
[35] T. Miloh, B. Spivak, A. L. Yarin, *J. Appl. Phys.* **2009**, *106*, 114910.
[36] O. O. Dosunmu, G. G. Chase, W. Kataphinan, D. H. Reneker, *Nanotechnology* **2006**, *17*, 1123.
[37] Z. Zhou, X. F. Wu, Y. Ding, M. Yu, Y. Zhao, L. Jiang, C. Xuan, C. Sun, *J. Appl. Polym. Sci.* **2014**, *131*, 40896.
[38] J. Holopainen, T. Penttinen, E. Santala, M. Ritala, *Nanotechnology* **2015**, *26*, 025301.
[39] X. F. Wu, Z. Zhou, O. Zholobko, J. J. Jenniges, B. Baatz, M. Ahmadi, J. Chen, *J. Appl. Phys.* **2020**, *127*, 054303.
[40] D. Lukas, A. Sarkar, L. Martinova, K. Vodsed'alkova, D. Lubasova, J. Chaloupek, P. Pokorny, P. Mikes, J. Chvojka, M. Komarek, *Textile Prog.* **2009**, *41*, 59.
[41] R. Nayak, R. Padhye, I. L. Kyratzis, Y. B. Truong, L. Arnold, *Textile Res. J.* **2011**, *82*, 129.
[42] J. S. Kim, D. H. Reneker, *Polym. Eng. Sci.* **1999**, *39*, 849.
[43] C. Kim, S. H. Park, W. J. Lee, K. S. Yang, *Electrochem. Acta* **2004**, *50*, 877.
[44] J. Weber, *ChemSusChem* **2010**, *3*, 181.
[45] H. Y. Li, Y. L. Liu, *J. Mater. Chem. A* **2013**, *1*(1), 1171.
[46] S. Jahangiri, I. Aravi, L. I. Şanli, Y. Z. Menceloğlu, E. Özden-Yenigün, *Polym. Adv. Technol.* **2018**, *29*, 594.
[47] T. Ibaraki, M. Tanaka, H. Kawakami, *Electrochim. Acta* **2019**, *296*, 1042.
[48] S. J. Cho, H. Choi, J. H. Youk, *Fibers Polym.* **2020**, *21*, 993.
[49] G. Sun, L. Kong, B. Liu, H. Niu, M. Zhang, G. Tian, S. Qi, D. Wu, *J. Membr. Sci.* **2019**, *582*, 132.
[50] M. S. Abdul-quadir, R. van der Westhuizen, W. Welthagen, E. E. Ferg, Z. R. Tshentu, A. S. Ogunlaja, *S. Afr. J. Chem.* **2019**, *72*, 88.
[51] F. F. F. Garrudo, R. N. Udangawa, P. R. Hoffman, L. Sordini, C. A. Chapman, P. E. Mikael, F. A. Ferreira, J. C. Silva, C. A. V. Rodrigues, J. M. S. Cabral, J. M. F. Morgado, F. C. Ferreira, R. Linhardt, *J. Mater. Today Chem.* **2019**, *14*, 100185.
[52] H. Penchev, F. Ublekov, D. Budurova, V. Sinigersky, *Mater. Lett.* **2017**, *187*, 89.
[53] M. L. Gardel, J. H. Shin, F. C. MacKintosh, L. Mahadevan, P. Matsudaira, D. A. Weitz, *Science* **2004**, *304*, 1301.
[54] M. Alava, K. Niskanaen, *Rep. Prog. Phys.* **2006**, *69*, 669.
[55] X. F. Wu, Y. A. Dzenis, *J. Appl. Phys.* **2005**, *98*, 093501.
[56] X. F. Wu, Y. A. Dzenis, *J. Appl. Phys.* **2007**, *102*, 044306.
[57] F. Chen, X. Peng, T. Li, S. Chen, X. F. Wu, D. H. Reneker, H. Hou, *J. Phys. D: Appl. Phys.* **2008**, *41*, 025308.
[58] X. F. Wu, Y. Y. Kostogorova-Beller, A. V. Goponenko, H. Q. Hou, Y. A. Dzenis, *Phys. Rev. E* **2008**, *78*, 061804.
[59] X. F. Wu, *J. Appl. Phys.* **2010**, *107*, 013509.
[60] X. F. Wu, A. Bedarkar, I. S. Akhatov, *J. Appl. Phys.* **2010**, *108*, 083518.
[61] X. F. Wu, Z. P. Zhou, W. M. Zhou, *Appl. Phys. Lett.* **2012**, *100*, 193115.
[62] Q. Shi, S. C. Wong, W. Ye, J. Hou, J. Zhao, J. Yin, *Langmuir* **2012**, *28*, 4663.
[63] J. Song, C. Chen, S. Zhu, M. Zhu, J. Dai, U. Ray, Y. Li, Y. Kuang, Y. Li, N. Quispe, Y. Yao, A. Gong, U. Leiste, H. A. Bruck, J. Y. Zhu, A. Vellore, H. Li, M. L. Minus, A. Martini, T. Li, L. Hu, *Nature* **2018**, *554*, 224.
[64] S. Deogekar, R. C. Picu, *J. Mech. Phys. Solids* **2018**, *116*, 1.
[65] S. Deogekar, M. R. Islam, R. C. Picu, *Int. J. Solid Struct.* **2019**, *169*, 194.
[66] M. Ahmadi, X. F. Wu, *J. Phys. Commun.* **2019**, *3*, 045001.
[67] M. Ahmadi, O. Zholobko, X. F. Wu, *Phys. Rev. E* **2020**, *102*, 013001.
[68] Y. Liao, R. Wang, M. Tian, C. Qiu, A. G. Fane, *J. Membr. Sci.* **2013**, *425*, 30.
[69] ASTM International, *ASTM D882-18 standard test method for tensile properties of thin plastic sheeting*, ASTM International, West Conshohocken, PA **2018**.
[70] K. J. Laidler, *J. Chem. Ed.* **1984**, *61*, 494.
[71] J. Richeton, S. Ahzi, L. Daridon, Y. Rémond, *J. Phys. IV France* **2003**, *110*, 39.
[72] Q. Yu, A. P. S. Selvadurai, *Philos. Mag.* **2007**, *87*, 3519.
[73] P. Hänggi, P. Talkner, *Rev. Modern Phys.* **1990**, *62*, 251.

How to cite this article: Zholobko O, Wu X-F, Zhou Z, Aulich T, Thakare J, Hurley J. A comparative experimental study of the hygroscopic and mechanical behaviors of electrospun nanofiber membranes and solution-cast films of polybenzimidazole. *J Appl Polym Sci*. 2020;137: e49639. https://doi.org/10.1002/app.49639